Quantized Soft-Decision-Based Compressive Reporting Design for Underlay/Overlay Cooperative Cognitive Radio Networks

Xiaoge Wu, *Graduate Student Member, IEEE*, Lin Zhang, *Senior Member, IEEE*, and Zhiqiang Wu, *Senior Member, IEEE*

***Abstract*—Cooperative spectrum sensing (CSS) systems use underlay or overlay strategies to identify underused or unused bands to achieve higher spectrum utilization. In hybrid underlay and overlay systems, spectrum sensing results may be sparse and a general reporting strategy is required to take multiple spectrum usage status into account. In this paper, we propose a general quantized soft decision (QSD) based compressive sensing and reporting strategy for hybrid systems. Our objective is to provide a general framework to report more reliable sensing results to improve the sensing precision and reduce the collision probability with the low complexity. To this end, the soft sensing decisions are quantized to multiple levels, then they are compressed and encoded, while the characteristic information of secondary users (SUs) including the index of the SUs, the interference tolerance level etc, is transmitted over equivalent bit channels. Furthermore, considering that different users may have different quality of service requirements, we propose four methods to allow SUs to deliver local sensing results with different precisions. Simulations are performed over additive white Gaussian noise (AWGN) and Rayleigh fading channels. The results validate the theoretical analysis, and demonstrate that our scheme effectively improves the sensing decision precision and reduces the collision probability.**

***Index Terms*—Hybrid overlay/underlay cognitive radio network, compressive and cooperative spectrum sensing, characteristic cooperation parameters, priority-based reporting, quantized-soft decisions, reliability.**

Manuscript received November 9, 2018; revised July 4, 2019 and September 25, 2019; accepted April 10, 2020. Date of publication April 17, 2020; date of current version September 9, 2020. This work was supported by the Key Research and Development and Transformation Plan of Science and Technology Program for Tibet Autonomous Region (No. XZ201901-GB-16), the open research fund from Shandong Provincial Key Lab. of Wireless Communication Technologies (No. SDKLWCT-2019-05), Guangdong Basic and Applied Basic Research Foundation (No. 2020A1515010703), the NSF grant (No. 1748494), Special fund for the development of local universities supported by the central finance of Tibet University in 2018 and the Project of National Natural Science Foundation of China (No. 61602531). The associate editor coordinating the review of this paper and approving it for publication was D. Cabric. *(Corresponding author: Lin Zhang.)*

Xiaoge Wu is with the School of Electronics and Information Technology, Sun Yat-sen University, Guangzhou 510006, China (e-mail: wuxiaogebaiying@qq.com).

Lin Zhang is with the School of Electronics and Information Technology, Sun Yat-sen University, Guangzhou 510006, China, and also with Shandong Provincial Key Laboratory of Wireless Communication Technologies, Jinan 250100, China (e-mail: isszl@mail.sysu.edu.cn).

Zhiqiang Wu is with the Department of Electrical Engineering, Tibet University, Lhasa 850012, China, and also with the Department of Electrical Engineering, Wright State University, Dayton, OH 45435 USA (e-mail: zhiqiang.wu@wright.edu).

Digital Object Identifier 10.1109/TCCN.2020.2988479

I. Introduction

IN COGNITIVE radio networks (CRN), the secondary user (SU) applies spectrum sensing technique to identify spectrum holes or available spectrum bands. Then using two types of access strategies [1], which are overlay and underlay, the SU transmits information over detected idle or underused bands without interfering with primary users (PU) [2]–[4].

Recently, cooperative spectrum sensing (CSS) [2], [3], [5] has been proposed for CRN, wherein the fusion center (FC) determines the spectrum usage status [6], based on the collected local sensing results reported from multiple SUs. Hence higher sensing precision can be achieved thanks to the cooperation between the SUs and the FC.

Since the FC makes decisions using the reported sensing results, the imperfect reporting channel conditions would degrade the spectrum sensing performances. Reference [7] investigates the performance of a multi-band CSS system and [8] evaluates the influences of reporting channel errors on the sensing precision when using a "majority-decision-aided" weighting rule. In addition, [9] studied the mean energy efficiency performances while [10] analyzed the cooperative sensing performances when imperfect reporting channels are not identical.

In order to further improve the spectrum usage decision precision and lower the complexity, research works have been done on the reporting strategy design for underlay/overlay CSS-aided CRN to get more precise spectrum usage status. In [6], the soft decision (SD) method is proposed to help FC to get more accurate spectrum usage status. In addition, in order to combat the imperfect reporting channel conditions, [11] presents an ON/OFF reporting mechanism where either signaling or remaining silent carries binary information to provide robust reporting over imperfect reporting channels. Moreover, [7] and [12] propose to reduce reporting errors to improve the sensing precision for multi-band CSS systems.

On the other hand, with the aim to lower the complexity, reference [13] proposed to compress the local decisions due to the sparsity of PU signal, and a hierarchical and adaptive spectrum sensing solution for overlay CRN is presented in [14]. In addition, reference [15] investigated the incorporation of rank-based censoring with CSS to reduce the transmission overhead of reporting channels in underlay CRN, while in [16], a random access protocol based reporting scheme is presented to reduce the complexity.

However, few research works have been done to investigate the CSS system using both underlay and overlay access strategies to identify underused and unused bands. Moreover, no general framework can be used for characterizing the multiple spectrum usage status which may allow different interference tolerance levels. Furthermore, the property that spectrum sensing results may be sparse is also not considered.

Different from the available research works which focus on the single underlay or overlay scenario, we study the hybrid underlay and overlay system which requires to characterize the multiple spectrum usage status. More explicitly, the novelty of this paper is that we propose to quantize the soft decision (QSD) of the spectrum usage, then a compressive polarized (QCP) method is proposed. Thus a general framework is constructed to report the spectrum sensing results with higher precisions.

In our design, local sensing results are quantized, then the QSDs are compressed to counteract the sparsity of the sensing results. Subsequently, in the reporting stage, the local sensing results are regarded as information bits, while SUs may transmit their own characteristics parameters, i.e., the SU index, interference tolerance level [17]–[19] and the occupied channel index flexibly based on the reporting channel quality and the user demands. More explicitly, in order to improve the reporting reliability, both the local sensing results and the characteristic parameters of SUs are encoded by the forward error correction (FEC) codes such as polar codes. We propose to flexibly encode the sensing results as information bits, while the characteristic parameters are totally or partially encoded as frozen bits based on the reporting channel quality and the decision precision demands of FC. Namely, considering that the users may have different quality requirements for the services, we present four methods to generate the frozen bits, which encode the whole or partial parts of characteristic parameters. Thus the collision probability that may happen during the sensing is potentially different, leading to different reliability performances.

Next, at the FC, the local decisions are recovered by applying the successive-cancellation (SC) algorithm [20] and nondestructive reconstruction. With the aid of the cooperation parameters, the collision probability can be lowered.

Furthermore, for the proposed QSD-based compressive polarized design we provide the theoretical performance analyses for the reliability and sensing performances, and compare the efficiency and complexity performances. We first apply heuristic method [20] to derive the theoretical upper and lower bound of the transmission error rate, then based on the Gaussian approximation (GA) method [21], we provide the error rate expression. As to the sensing performance, we present the overall detection probability and collision probability expressions. Subsequently, we present a definition of effective spectral efficiency (ESE) to measure the transmission efficiency performances, followed by the complexity analysis and comparisons.

At last, simulations are performed over additive white Gaussian noise (AWGN) and slow flat-fading Rayleigh channels, and the results verify the theoretical analysis, and demonstrate the outstanding performances of our scheme for underlay/overlay cooperative CRN.

Briefly, the main contributions of this paper are:

1) We present a general QSD-based sensing for hybrid underlay and overlay CRN. Different from the available research achievements, which only consider the pure underlay or overlay scenario, in our design, the soft decision of the spectrum usage is quantized. Thus, the adjustable quantization levels allow the CRN nodes to deliver the local sensing results with different precision no matter the access mode is underlay or overlay.
2) We propose to compress the QSD to improve the transmission efficiency and to lower the complexity with considerations of the sparsity of the sensing results. The compressive transmissions effectively counteract the sparsity of the spectrum sensing, whereby the redundancy is reduced.
3) We propose to deliver the characteristic parameters of SUs to the FC flexibly as information bits or frozen bits when applying polar coding, which depends on the reporting channel quality and the spectrum usage decision precision demands of FC. Thus the reporting quality can be improved with no extra bandwidth is required.
4) Different from other report design, which only transmit the local sensing results to FC, in our design, both the local sensing results and the characteristic parameters of SUs are transmitted to FC to provide more information for improving the precision of spectrum usage decisions.
5) For the considered practical hybrid underlay and overlay system, we analyze the theoretical reliability, sensing and efficiency performances as well as the complexity. Based on GA method and Heuristic method, we derive the error rate and the bound. Then we analyze the overall detection and collision probability. Subsequently, we present a definition of ESE to measure how many local sensing results are transmitted and provide the complexity analysis.

The rest of the paper is organized as follows. Section II provides the system model of CSS CRNs. Then, Section III provides the details of the QCP based CSS system, including the quantized sensing results composition, encoding procedures of sensing results and the characteristic information of SUs, and the decision making of FCs. In Section IV we present the theoretical analysis of the system's performance, which is verified by simulation results in Section V. Finally, we conclude our findings and discuss the future research direction in Section VI.

II. The CSS System

In this section, we will describe the CSS system model.

Fig. 1 illustrates the CSS-aided CRN model with M SUs $\{\mathrm{C}_1, \ldots, \mathrm{C}_M\}$ and 1 FC. In this system, SUs detect Q subbands and provide local sensing results using the proposed QSD method, then report the sensing results and their own characteristic information to the FC. The FC collects the information obtained from multiple SUs and determines the spectrum usage status.

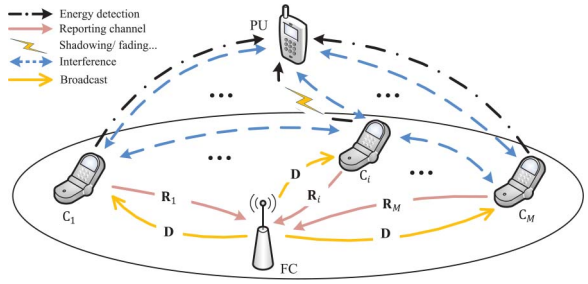

Fig. 1. System model.

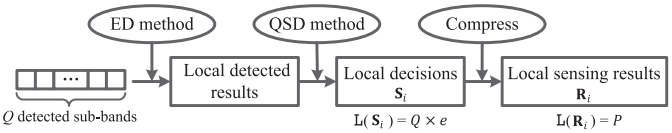

Fig. 2. The general QSD compressive framework for hybrid underlay and overlay system.

Notably, considering that SUs are isolated in the space and perform sensing independently [3], without loss of the generality, we assume that the local spectrum sensing results are statistically independent. Meanwhile, since the reporting channel is in fact a logical channel and can be divided into multiple sub-feedback channels [16], without loss of generality, we can assume the reporting process is different from each other. Additionally, as shown in Fig. 1, the imperfect channel conditions of practical wireless channels such as correlated transmissions may induce interferences to the transmitted signals among neighbouring SUs. However, it is worth mentioning that the imperfect wireless channel conditions such as correlated transmissions will not influence the independence of the local sensing results or the reporting channels.

III. The QCP-Based CSS Scheme

In this section, we will present the details of the general compressive QSD framework for hybrid underlay and overlay CSS system and the reporting design.

A. The General Local Sensing Framework for Hybrid Underlay and Overlay CSS System

Each SU applies energy detection (ED) method, which has the lowest complexity [2], to detect sub-bands. As shown in Fig. 2, for SU C_i, $i \in \{1, 2, \ldots, M\}$, we use QSD method to generate the decision for the j-th sub-band, $j \in \{1, 2, \ldots, Q\}$, which is denoted by $\mathbf{s}_i^{(j)}$ for hybrid underlay and overlay CRNs. The local sensing result for all Q subbands is denoted by $\mathbf{S}_i = [\mathbf{s}_i^{(1)}, \mathbf{s}_i^{(2)}, \ldots, \mathbf{s}_i^{(Q)}]$ and compressed to counteract the sparsity of PU signals. The resultant $\mathbf{R}_i$ is then reported to FC.

1) Generation of $\mathbf{s}_i^{(j)}$*:* Fig. 3 illustrates three methods to generate $\mathbf{s}_i^{(j)}$, which are hard decision (HD), SD and QSD method. It can be seen that in the HD method, $\mathbf{s}_i^{(j)}$ is determined as a binary bit 0 or 1, which can only be used in the overlay scenario. The SD method provides the probability estimation for $\mathbf{s}_i^{(j)}$, which can be used in overlay and underlay CRNs. However, this method has high computational complexity [6].

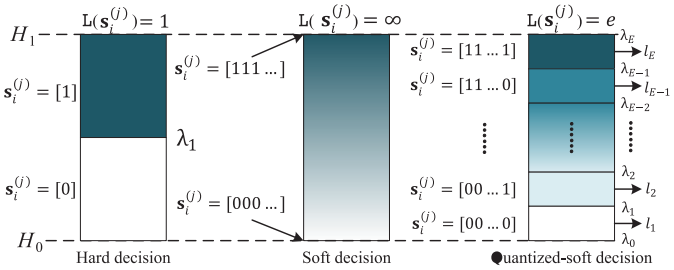

Fig. 3. Three different decision methods for local spectrum sensing.

Here, we propose to use the QSD to build a general framework to provide $\mathbf{s}_i^{(j)}$ for both underlay and overlay systems. Namely, in these two systems, local spectrum sensing results are compressed and quantized to multiple levels to represent the spectrum usage status. More details are given as below.

Underlay CRN: In this scenario, SUs and PU can transmit simultaneously in a sub-band with the interference constraints for PU and quality of service (QoS) constraints for SUs. For the i-th SU C_i, let $f_i(\cdot)$ denote the probability density function (pdf) of the detected energy, $f_i(\cdot|H_0)$ and $f_i(\cdot|H_1)$ denote the pdfs of the detected energy when PU signal absents and exists respectively. Then $f_i(\cdot)$ can be expressed as

$$f_i(\cdot) = f_i(\cdot|H_0)(1 - \beta_{PU}) + f_i(\cdot|H_1)\beta_{PU} \tag{1}$$

where β_{PU} is the ratio of sub-bands occupied by PU [6].

Using the maximum output entropy quantization scheme [22], we divide the ED results into E levels, where $E = 2^e$, $e \in \mathbb{Z}^+$. Let $\lambda = \{\lambda_0, \ldots, \lambda_E\}$ denote the thresholds for the quantization region, $l = \{l_1, \ldots, l_E\}$ denote quantization levels, then we have $\mathbf{s}_i^{(j)} \in l$. The probability mass function (pmf) value of quantization level l_t, $t \in \{1, 2, \ldots, E\}$ is equal to $1/E$. Assuming $\lambda_0 = -\infty$, $\lambda_E = \infty$, and l_t is the centroid between λ_{t-1} and λ_t, then based on Eq. (1), we have

$$l_t = \frac{\int_{\lambda_{t-1}}^{\lambda_t} x f_i(x)\,dx}{\int_{\lambda_{t-1}}^{\lambda_t} f_i(x)\,dx} = E\int_{\lambda_{t-1}}^{\lambda_t} x f_i(x)\,dx. \tag{2}$$

For the j-th sub-channel, C_i can decide $\mathbf{s}_i^{(j)}$ as l_t by comparing the detected energy and the quantization threshold. Based on Eq. (2), the pmf value for $\mathbf{s}_i^{(j)}$ can be written as:

$$P\left(\mathbf{s}_i^{(j)} = l_t\right) = \int_{\lambda_{t-1}}^{\lambda_t} f_i(x)\,dx = \frac{1}{E}. \tag{3}$$

Moreover, let $\mathtt{L}(\cdot)$ denote the length of the specific sequence, the length of $\mathbf{s}_i^{(j)}$ can be expressed as $\mathtt{L}(\mathbf{s}_i^{(j)}) = e$, and for all Q subbands, we have $\mathtt{L}(\mathbf{S}_i) = Q \times e$.

Overlay CRN: In the overlay scenario, the SU transmits over the sub-band where PU signal is detected as being absent. The local decision is "0"/"1", which represents PU signal absent or existing respectively. In our proposed structure, when $e = 1$, the QSD method simplifies as a HD method, which has low complexity and can be generally used in the overlay CRN.

Therefore, $\mathbf{s}_i^{(j)}$ can be used to represent the spectrum usage status for hybrid underlay and overlay CSS systems, and the parameter e can be adjusted to achieve a tradeoff between the sensing precisions and the computational complexities.

2) Generation of $\mathbf{R}_i$*:* Subsequently, we further compress $\mathbf{S}_i$ to improve the efficiency. According to [23], [24], since PU signal is sparse in CRN, we can compress $\mathbf{S}_i$ as

$$\mathbf{R}_i = \mathbf{S}_i \Theta \tag{4}$$

where Θ is a measurement matrix, $\Theta \in \mathbb{R}^{\mathtt{L}(\mathbf{S}_i)\times P}$ [13], and $\mathtt{L}(\mathbf{R}_i) = P$, $P < \mathtt{L}(\mathbf{S}_i)$. Note that based on Eq. (4), the complexity of evaluating $\mathbf{R}_i$ is determined by operations of Θ, which is $O(\mathtt{L}(\mathbf{S}_i)\log \mathtt{L}(\mathbf{S}_i))$ [25]. Then $\mathbf{R}_i$ is transmitted by C_i to FC.

B. Sensing Reports Transmission

As mentioned above, the sensing results $\mathbf{R}_i$ are regarded as information bits, while the characteristic information of C_i is flexibly treated as information bits or redundancy bits according to the FC demands. Then both $\mathbf{R}_i$ and C_i are encoded by FEC codes such as polar codes. Take polar encoding $\mathbf{G}_N$ as an example [20]. Let K, A, A^c denote the information bits number, the set of information bits indices and the frozen bits, respectively, then we have $N = 2^n$, where $n \in \mathbb{Z}^+$.

1) Characteristic Information Processing: According to [20], the frozen bits are taken as 0 in general and do not carry any information, which leads to transmission efficiency degradation.

Taking different low consumption requirements or power limited properties of the sensing nodes into considerations, we propose to embed the characteristic information of the SU C_i, including the SU index i, the interference tolerance level o_i [18], and the accessed sub-band index a_i, partially or totally as the frozen bits to reduce collisions. Note that each o_i can be generated from quantizing the different SU equipment parameter.

As shown in Fig. 4, the characteristic information of C_i is encoded as frozen bits. Define $\mathtt{D2B}(\cdot)$ as an operation that converts a decimal number into the binary form. Then based on different FC demands, for each C_i, we could use the whole characteristic information or a part of characteristic information to generate frozen bits $\mathbf{u}_{A^c}^{(i)}$. Let $\zeta_\star$ $\star \in \{1,2,3,4\}$ denote the Scheme 1-4 listed above. Namely, we have

- Scheme 1 (ζ_1): Embed all characteristic information, i.e., i, o_i, a_i in frozen bits. As shown in Fig. 4(a), we have $\mathbf{u}_{A^c}^{(i)} = [\mathtt{D2B}(i), \mathtt{D2B}(o_i), \mathtt{D2B}(a_i)]$, then $K = \mathtt{L}(\mathbf{R}_i)$.
- Scheme 2 (ζ_2): Embed one characteristic information in frozen bits. For example, as shown in Fig. 4(b), we embed a_i in frozen bits, transmit o_i, i via information bits, we have $\mathbf{u}_{A^c}^{(i)} = [\mathtt{D2B}(i), \mathtt{D2B}(o_i)]$, then $K = \mathtt{L}(\mathbf{R}_i) + \mathtt{L}(\mathtt{D2B}(a_i))$.
- Scheme 3 (ζ_3): Embed two characteristic information in frozen bits. For example, as shown in Fig. 4(c), we embed a_i, o_i in frozen bits, transmit i via information bits, we have $\mathbf{u}_{A^c}^{(i)} = [\mathtt{D2B}(i)]$, then $K = \mathtt{L}(\mathbf{R}_i) + \mathtt{L}(\mathtt{D2B}(a_i)) + \mathtt{L}(\mathtt{D2B}(o_i))$.

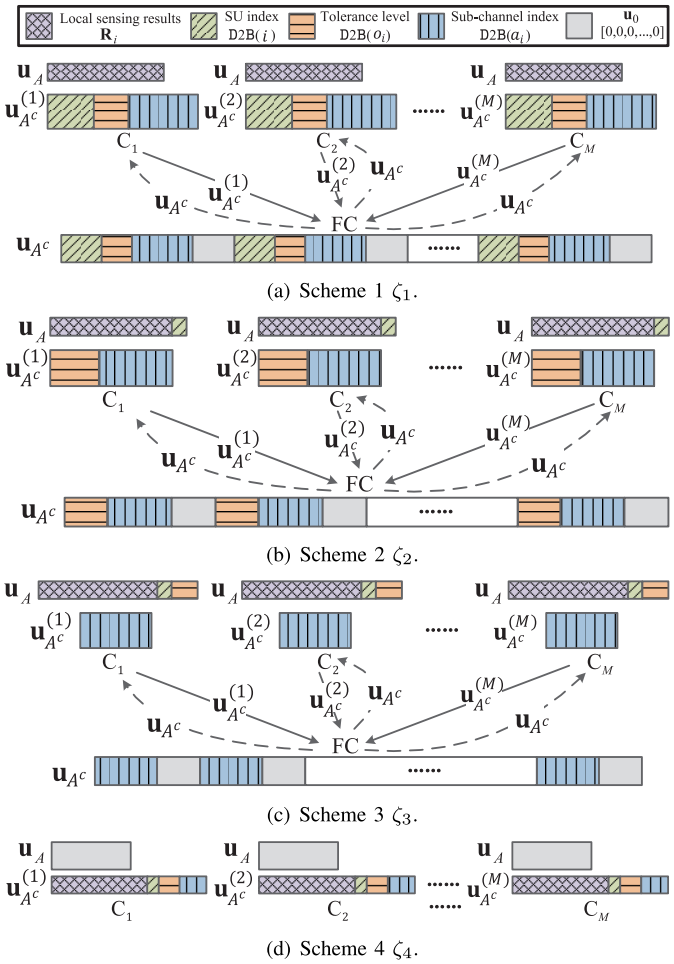

Fig. 4. Generation of the frozen bits.

- Scheme 4 (ζ_4): Directly transmit all characteristic information in information bits. As shown in Fig. 4(d), i, o_i, a_i are transmitted via information bits. In this case, we have $K = \mathtt{L}(\mathbf{R}_i) + \mathtt{L}(\mathtt{D2B}(i)) + \mathtt{L}(\mathtt{D2B}(o_i)) + \mathtt{L}(\mathtt{D2B}(a_i))$. Meanwhile, $\mathbf{u}_{A^c}^{(i)} = \mathbf{u}_{A^c}$, which are set as $\mathbf{u}_0 = [0,0,\ldots,0]$, $\mathtt{L}(\mathbf{u}_0) = N - K$.

Notably, in the schemes of ζ_1, ζ_2 and ζ_3, SUs delivered their own $\mathbf{u}_{A^c}^{(i)}$ to FC, then FC collects and broadcasts $\mathbf{u}_{A^c}$, which is represented as $\mathbf{u}_{A^c} = [\mathbf{u}_{A^c}^{(1)}, \mathbf{u}_0, \ldots, \mathbf{u}_{A^c}^{(M)}, \mathbf{u}_0]$, where $\mathtt{L}(\mathbf{u}_0) = \frac{N-K}{M} - \mathtt{L}(\mathbf{u}_{A^c}^{(i)})$. In ζ_4, there is no requirement for the SU C_i to deliver the $\mathbf{u}_{A^c}^{(i)}$ to FC.

2) Local Sensing Report Transmission: In addition, the SU C_i transmits local sensing reports by encoding the local sensing results $\mathbf{R}_i$ based on the $\mathbf{G}_N$-encoding parameters $(N, K, A, \mathbf{u}_{A^c})$. Let $\mathbf{u}_i$ denote the code that contains $\mathbf{u}_A$ and $\mathbf{u}_{A^c}$, which are generated using the Scheme 1-4 given by Fig. 4, then the encoded data $\mathbf{x}_i$ can be expressed as [20]:

$$\mathbf{x}_i = \mathbf{u}_i \mathbf{G}_N = \mathbf{u}_A \mathbf{G}_N(A) \oplus \mathbf{u}_{A^c} \mathbf{G}_N(A^c) \tag{5}$$

where $\mathtt{L}(\mathbf{x}_i) = N$, $\mathbf{G}_N$ is a $(N \times N)$ generation matrix. $\mathbf{G}_N(A)$ and $\mathbf{G}_N(A^c)$ are the sub-matrices which consist of the row vectors of $\mathbf{G}_N$ selected by A and A^c, respectively.

Define $\oplus$ operator as the modulo-2 addition, then we have

$$\mathbf{G}_N = \mathbf{B}_N \mathbf{F}^{\otimes n} = \mathbf{J}_N \left(\mathbf{I}_2 \otimes \mathbf{B}_{N/2} \right) \mathbf{F}^{\otimes n} \tag{6}$$

where $\otimes$ is the Kronecker product operator, $\mathbf{I}_2$ is the (2×2) identity matrix, $\mathbf{J}_N$ is a permutation operation that performs [20]

$$(1, 2, 3, \ldots, N) \rightarrow (1, 3, \ldots, N-1, 2, 4, \ldots, N) \tag{7}$$

and $\mathbf{B}_N$ takes a recursive form as

$$\mathbf{B}_N = \mathbf{J}_N \left(\mathbf{I}_2 \otimes \mathbf{B}_{\frac{N}{2}} \right) = \mathbf{J}_N (\mathbf{I}_2 \otimes \cdots (\mathbf{J}_4 (\mathbf{I}_2 \otimes \mathbf{B}_2))) \tag{8}$$

where $\mathbf{B}_2 = \mathbf{I}_2$. Furthermore, the operator $\mathbf{F}^{\otimes n}$ in (6) is defined by

$$\mathbf{F}^{\otimes n} = \underbrace{\mathbf{F} \otimes \mathbf{F} \otimes \cdots \otimes \mathbf{F}}_{n} \tag{9}$$

where $\mathbf{F} = \left[\begin{smallmatrix} 1 & 0 \\ 1 & 1 \end{smallmatrix} \right]$.

Subsequently, we transmit the encoded bit $\mathbf{x}_i$ over the reporting channel.

C. Decision Making of FC

Let $\mathbf{y}_i$ denote the received data at the FC, we here use the SC algorithm [26] to decode $\mathbf{y}_i$. The SC decoder estimates $\mathbf{u}_i$ as $\hat{\mathbf{u}}_i$ by observing $(\mathbf{y}_i, \mathbf{u}_{A^c})$. Let $\hat{\mathbf{u}}_i = [\hat{u}_i(1), \hat{u}_i(2), \ldots, \hat{u}_i(N)]$, $\mathbf{y}_i = [y_i(1), y_i(2), \ldots, y_i(N)]$. For $b = 1, 2, \ldots, N$, if $b \in A^c$, set $\hat{u}_i(b) = y_i(b)$, if $b \in A$, The FC determines the value of $\hat{u}_i(b)$ based on previous decisions $\hat{\mathbf{u}}_i^{b-1} = [\hat{u}_i(1), \ldots, \hat{u}_i(b-1)]$.

To be more explicit, the likelihood ratio (LR) [20] is calculated by

$$L_N^{(b)} \left(\mathbf{y}_i, \hat{\mathbf{u}_i}^{b-1} \right) = \frac{W_N^{(b)} \left(\mathbf{y}_i, \hat{\mathbf{u}_i}^{b-1} | 0 \right)}{W_N^{(b)} \left(\mathbf{y}_i, \hat{\mathbf{u}_i}^{b-1} | 1 \right)} \tag{10}$$

where $W_N^{(b)}(\cdot)$ is the transition probability function. Then FC can get the estimation results $\hat{\mathbf{R}}_i$ based on $\hat{\mathbf{u}}_i$, $\mathtt{L}(\hat{\mathbf{R}}_i) = \mathtt{L}(\mathbf{R}_i)$.

Subsequently, FC reconstructs the compressive sensing results based on $\hat{\mathbf{R}}_i$. According to [13], the reconstruction process can be formed as a convex optimization problem as follows [25]

$$\min \quad \left\| \hat{\mathbf{S}}_i \right\|_1 \tag{11}$$

$$\text{s.t.} \quad \hat{\mathbf{R}}_i = \hat{\mathbf{S}}_i \Theta \tag{12}$$

where the constraint $\hat{\mathbf{R}}_i = \hat{\mathbf{S}}_i \Theta$ indicates that the reconstruction is nondestructive. Eq. (11) can be solved by the basis pursuit (BP) algorithm [25], which is one of an effective convex relaxation method to reconstruct the compressed signal. Thus the signal can be reconstructed with a small number of observations.

It is worth mentioning that the encoding and the SC decoding have the same computational complexity of $O(N \log_2 N)$ [20], the decoding latency is $2(N-1)$ clock cycles [26], while the complexity of BP algorithm is $O(\mathtt{L}(\mathbf{S}_i)^3)$ [25].

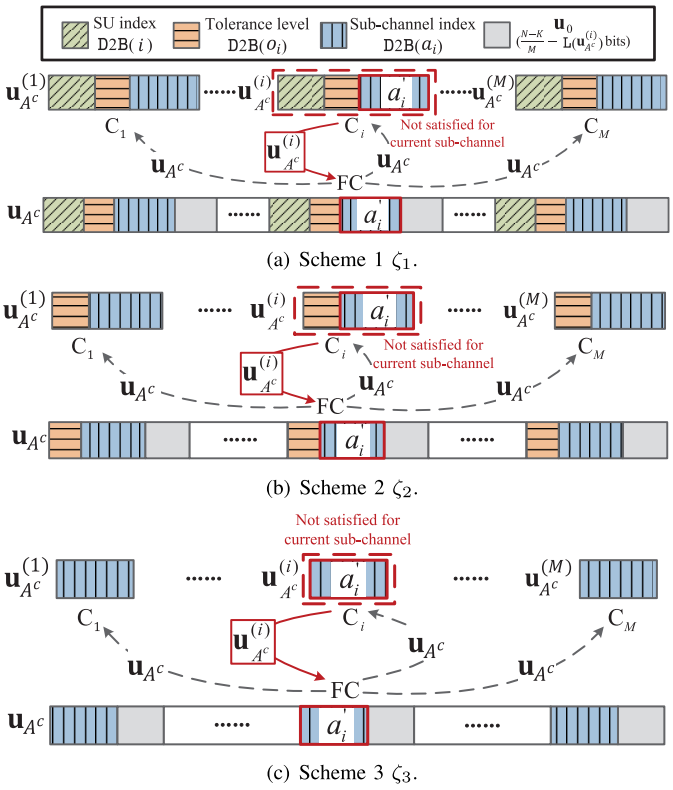

Fig. 5. Generation of the new frozen bits.

Define $\mathtt{B2D}(\cdot)$ as an operation that converts a binary number into the decimal form. For the j-th sub-band, FC combines $\hat{\mathbf{S}}_i = [\hat{\mathbf{s}}_i^{(1)}, \ldots, \hat{\mathbf{s}}_i^{(Q)}]$ from C_i and decides the spectrum usage status as

$$\mathbf{D}_j = \mathtt{D2B} \left(\frac{1}{M} \sum_{i=1}^{M} \mathtt{B2D} \left(\hat{\mathbf{s}}_i^{(j)} \right) \right) \tag{13}$$

where $\mathtt{L}(\mathbf{D}_j) = \mathtt{L}(\hat{\mathbf{s}}_i^{(j)}) = e$. Then FC broadcasts the final decision $\mathbf{D} = [\mathbf{D}_1, \mathbf{D}_2, \ldots, \mathbf{D}_Q]$ to all SUs.

D. Spectrum Access Strategy of SUs

Based on the received final decision $\mathbf{D}$ delivered by FC, SUs will determine whether to access the available sub-bands to avoid collisions. For example, when $i \in \{1, 2, \ldots, M\}$, for a sub-band with the index a_i, $a_i \in \{1, 2, \ldots, Q\}$, according to $\mathbf{D}$, if $o_i \geq \mathbf{D}_{a_i}$, i.e., the interference is tolerable, then C_i can get permitted to access this sub-band. By contrast, if $o_i < \mathbf{D}_{a_i}$, C_i will select a new sub-band with index a_i' which satisfying $\mathbf{D}_{a_i'} \leq o_i$.

In order to reduce collisions, the characteristic information contained in $\mathbf{u}_{A^c}$ is utilized. More explicitly, as shown in Fig. 5, in Scheme ζ_1, ζ_2 and ζ_3, we have $a_i' \neq a_{i_o}$, $i, i_o \in \{1, 2, \ldots, M\}$ and $i \neq i_o$, where a_{i_o} can be obtained in $\mathbf{u}_{A^c}$. Then $\mathbf{u}_{A^c}$ is updated to FC to reduce collisions. Note that there is no requirement for SU to update $\mathbf{u}_{A^c}$ to FC in ζ_4 since it does not embed the characteristic information in frozen bits, which is also shown in Fig. 4(d).

IV. Theoretical Performance Analysis

In this section, for the hybrid underlay and overlay CSS system, we analyze the theoretical performances, including the transmission error rate, the overall detection probability, and the collision probability in CRNs.

A. The Transmission Performance

We neglect the compression errors due to the nondestructive reconstruction at the FC, the sensing performance is thus mainly determined by the transmission performance.

For C_i and the *j*-th sub-band, assume the FC recovers $\hat{\mathbf{s}}_i^{(j)}$ using the received $\mathbf{y}_i$. The transmission errors may cause the distribution of $\hat{\mathbf{s}}_i^{(j)}$ to differ from that of $\mathbf{s}_i^{(j)}$. Then under hypotheses that H_*, $* \in \{0,1\}$, the pmf of $\hat{\mathbf{s}}_i^{(j)}$ can be calculated by

$$P\left(\hat{\mathbf{s}}_i^{(j)} \mid H_*\right) = \sum_{t=1}^{E} (P_e)^{\mu} (1-P_e)^{e-\mu} P\left(\mathbf{s}_i^{(j)} = l_t \mid H_*\right) \tag{14}$$

where μ is the Hamming distance between $\mathbf{s}_i^{(j)}$ and $\hat{\mathbf{s}}_i^{(j)}$. For the *i*-th SU, P_e denotes the polarized transmission error rate of $\mathbf{u}_i$, which can be calculated by

$$P_e = \prod_{k=1;\hat{\mathbf{u}}_i(k)\neq \mathbf{u}_i(k)}^{K} P(\hat{\mathbf{u}}_i(k) \mid \mathbf{u}_i(k)) \tag{15}$$

where $P(\hat{\mathbf{u}}_i(k)|\mathbf{u}_i(k))$ is a conditional probability function of $\hat{\mathbf{u}}_i(k)$. Note that in Eq. (15), based on the principle of channel polarization, we assume that each bit $\mathbf{u}_i(k)$ in $\mathbf{u}_i$ is transmitted in the polarized bit-channel independently.

Moreover, for polar codes, we can calculate the mathematical transmission error rate expressions based on Heuristic method [20] and the GA method [21]. Notably, the Rayleigh fading channel can be transformed into an equivalent AWGN channel with the same average mutual information (AMI) [21], therefore, in the following analysis, we will take AWGN channel as an example, and analyze the theoretical transmission error rate.

1) Heuristic Method Based Error Rate Analysis: In the Heuristic method, according to [20], the channel polarization refers to the fact that we could possibly synthesize a second set of *N* binary-input channels $\{W_N^{(b)} : 1 \le b \le N\}$ out of *N* independent copies of a given B-DMC *W*.

Given a channel *W*, there are two important parameters: the symmetric capacity *I*(*W*) and the Bhattacharyya parameter *Z*(*W*), which are used to measure the rate and the reliability, respectively. *Z*(*W*) is the upper bound for the probability of the decision error when 0 or 1 is transmitted over *W* for one time, which can be expressed as:

$$Z(W) \triangleq \sum_{y\in\mathcal{Y}} \sqrt{W(y \mid 0)\, W(y \mid 1)}. \tag{16}$$

Subsequently, $Z(W_N^{(b)})$ can be used to measure the error performance of a bit channel $W_N^{(b)}$. By selecting $Z(W_N^{(b)})$ with a smaller value, we can choose the noiseless channels, while the Bhattacharyya parameter can be calculated by [20]

$$Z\left(W_N^{(2j_n-1)}\right) = 2Z\left(W_{N/2}^{(j_n)}\right) - \left(Z\left(W_{N/2}^{(j_n)}\right)\right)^2 \tag{17}$$

$$Z\left(W_N^{(2j_n)}\right) = \left(Z\left(W_{N/2}^{(j_n)}\right)\right)^2 \tag{18}$$

where $Z(W_1^{(1)})$ depends on the channel *W*, $j_n \in \{1,2,\ldots,\frac{N}{2}\}$. For the AWGN channel, *W* is characterized by the SNR denoted by ω. We have:

$$Z\left(W_1^{(1)}\right) = e^{-\frac{\omega}{2}}. \tag{19}$$

Then $Z(W_N^{(b)})$ can be calculated based on Eq. (17)-Eq. (19). According to [27], denote P_e^U and P_e^L as the upper and lower bounds of the transmission error rate respectively, which can be calculated by

$$P_e^U = \max_{b\in A} Z\left(W_N^{(b)}\right) \tag{20}$$

$$P_e^L = \frac{1}{K}\sum_{b\in A} Z\left(W_N^{(b)}\right) \tag{21}$$

where *A* is the index set of information bits.

2) GA Method Based Error Rate Analysis: Considering that in practical wireless systems, the number of the transmitted bit is large, hence we can apply the GA method, which employs Gaussian distribution to approximate the statistical characteristics of the information. More explicitly, for the AWGN channel *W* with the variance of σ^2, then the LR message over the channel *W* is Gaussian distributed with the mean $\frac{2}{\sigma^2}$ and variance $\frac{4}{\sigma^2}$.

Based on the probability density function (pdf) of $L_N^{(b)}$ which can be obtained through Eq. (10), the corresponding mean $m_N^{(b)}$ can be computed recursively by

$$m_N^{(2j_n-1)} = f^{-1}\left(1-\left(1-f\left(m_{N/2}^{(j_n)}\right)^2\right)\right) \tag{22}$$

$$m_N^{(2j_n)} = 2m_{N/2}^{(j_n)} \tag{23}$$

where $m_1^{(1)} = \frac{2}{\sigma^2}$, and $f(\cdot)$ denotes the function, which calculates the mean of LR on check nodes and variable nodes for low density parity check code (LDPC) using the GA method [21], expressed as

$$f(x) = 1 - \frac{1}{\sqrt{4\pi x}}\int_{-\infty}^{\infty} \tanh\left(\frac{\theta}{2}\right)\exp\left[-\frac{-(\theta-x)^2}{4x}\right]\mathrm{d}\,\theta. \tag{24}$$

For each bit-channel $W_N^{(b)}$, the pdf is estimated under the assumption that the previous bits are decoded correctly. Thus, as proved in [21], the probability that an error occurs in the bit-channel $W_N^{(b)}$ can be calculated by

$$P_e\left(W_N^{(b)}\right) = \frac{1}{2}erfc\left(\frac{1}{2}\sqrt{m_N^{(b)}}\right) \tag{25}$$

where $erfc(x) = \frac{2}{\sqrt{\pi}}\int_x^{\infty} e^{-\rho}\,\mathrm{d}\,\rho$.

Let P_e^{GA} represent the transmission error rate calculated by GA method, we obtain

$$P_e^{GA} = 1 - \prod_{b \in A} P_e\Big(W_N^{(b)}\Big). \tag{26}$$

It is worth pointing out that the analysis presented above can be further extended for the error rate evaluation of our design over the Rayleigh fading channel, which is equivalent to the analysis over AWGN channel with the same average mutual information (AMI) [21].

Note that in the GA method based analysis, the complexity is mainly determined by Eq. (22) while the complexity of Eq. (23) can be neglected. Nevertheless, we can reduce the computational complexity of Eq. (22) by approximating the function $f(\cdot)$ as below [21]

$$f(x) = \begin{cases} e^{\alpha x^{\psi} + \varpi}, & x < 10 \\ \sqrt{\frac{\pi}{x}} e^{-\frac{x}{4}}\big(1 - \frac{10}{7x}\big), & x \geq 10 \end{cases} \tag{27}$$

where $\alpha = -0.4527$, $\varpi = 0.0218$ and $\psi = 0.86$.

B. The Overall Detection Probability and Collision Probability

In the fusion process, the FC make final decisions about the usage state for the sub-channels based on the received local sensing results, which are independently generated by different SUs. Due to the spacial diversity of SUs, we assume the local sensing results are statistically independent from each other [2]. Then we can derive the statistical distribution of the test Φ_j based on Eq. (14) as

$$\Phi_j = \sum_{i=1}^{M} \log \frac{P\Big(\hat{\mathbf{s}}_i^{(j)} | H_1\Big)}{P\Big(\hat{\mathbf{s}}_i^{(j)} \,|\, H_0\Big)}. \tag{28}$$

Given the overall false alarm probability Q_f, let η_j and γ_j denote the threshold of overall decision and the randomization parameter, which can be calculated by [6]

$$\eta_j = \min\big\{x : P\big(\Phi_j > x \,|\, H_0\big) < Q_f\big\} \tag{29}$$

$$\gamma_j = \frac{Q_f - P\big(\Phi_j > \eta_j \,|\, H_0\big)}{P\big(\Phi_j = \eta_j \,|\, H_0\big)}. \tag{30}$$

Then applying the Neyman-Pearson test [6], we decide the spectrum usage states as

- H_0, when $\Phi_j < \eta_j$.
- H_1 with probability γ_j, when $\Phi_j = \eta_j$.
- H_1, when $\Phi_j > \eta_j$.

The overall detection probability Q_d is obtained as:

$$Q_d = \frac{1}{Q} \sum_{j=1}^{Q} \big[P\big(\Phi_j > \eta_j \,|\, H_1\big) + \gamma_j P\big(\Phi_j = \eta_j \,|\, H_1\big)\big]. \tag{31}$$

Finally, we can obtain the collision probability P_c, which is the probability of accessing the occupied spectrum, as

$$P_c = \frac{1}{M} \sum_{i=1}^{M} [P(\Phi_{a_i} \leq \eta_{a_i} \,|\, H_1)]. \tag{32}$$

TABLE I
THE SPECTRAL EFFICIENCY AND COMPLEXITY OF DIFFERENT LOCAL SENSING REPORTING SCHEMES

Case ($\Im$)	Case 1 ($\Im_1$)	Case 2 ($\Im_2$)	Case 3 ($\Im_3$)
Scheme	QSD + Polar coding	QSD + Compression + Polar coding	QSD + Compression + $\zeta_\star$ based polar coding
Coding rate for the same N	$\frac{Q\times e}{N}$	$\frac{P}{N}$	$\frac{K_{\zeta_\star}}{N}$
Coding rate comparison for the same N	$\Im_1 > \Im_3(\zeta_4) > \Im_3(\zeta_3) > \Im_3(\zeta_2) > \Im_3(\zeta_1) = \Im_2$		
Effective spectral efficiency, η_{ese}	$\frac{B_w}{Q\times e}$	$\frac{B_w}{P}$	$\frac{B_w}{K_{\zeta_\star}}$
Effective spectral efficiency comparison	$\Im_1 < \Im_3(\zeta_4) < \Im_3(\zeta_3) < \Im_3(\zeta_2) < \Im_3(\zeta_1) = \Im_2$		
Coding Complexity for the same coding rate r	$O(\frac{Q\times e}{\log \frac{Q\times e}{r}})$	$O(\frac{P}{r}\log\frac{P}{r})$	$O(\frac{K_{\zeta_\star}}{r}\log\frac{K_{\zeta_\star}}{r})$
Coding Complexity comparison for the same coding rate r	$\Im_1 > \Im_3(\zeta_4) > \Im_3(\zeta_3) > \Im_3(\zeta_2) > \Im_3(\zeta_1) = \Im_2$		

C. Effective Spectral Efficiency and Complexity

In this subsection, we will analyze and compare the efficiency and complexity of the proposed QCP-CSS schemes. It is worth pointing out that different from the traditional spectral efficiency definition, here we present a definition of ESE to measure the efficiency performance of our design.

Specifically, following the similar principle of defining the traditional spectral efficiency, wherein the information bits are regarded as the effective information and the spectral efficiency is measured in terms of the code rate, we here present an ESE definition to measure how many local detection results could be transmitted within the specific bandwidth.

Let η_{ESE} denote the ESE, B_w represent the bandwidth of a given spectrum band, s_{inf} represent the effective information bits used to carry the information of the local detection results of Q different sub-bands, and $K(s_{inf})$ denote the number of effective information bits. Then we define the ESE as

$$\eta_{ESE} = \frac{B_w}{K\big(s_{inf}\big)}. \tag{33}$$

Subsequently, based on the proposed ESE definition, we compare the code rate, the ESE and the complexity of our design in Table I in three cases of local sensing results transmissions, which are represented by $\Im_1$, $\Im_2$ and $\Im_3$. More explicitly, in Case 1 ($\Im_1$), we only use the QSD method and polar coding for reports processing, then in Case $\Im_2$, we add the compression process, while in Case 3 ($\Im_3$), we apply the QCP-CSS scheme based on different characteristic information processing schemes $\zeta_\star$, $\star \in \{1, 2, 3, 4\}$.

To elaborate a bit further, let $K_{\zeta_\star}$ denote the length of information bits when applying the scheme $\zeta_\star$, then we have

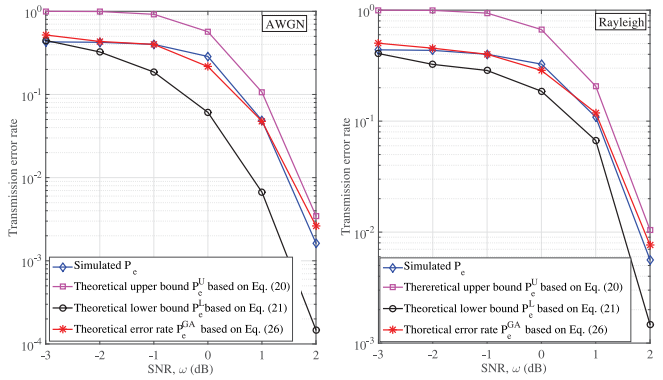

Fig. 6. Simulated and theoretical error rate performances evaluated by our derived Eq. (20), (21) and (26) respectively when applying the proposed QCP-CSS scheme 1.

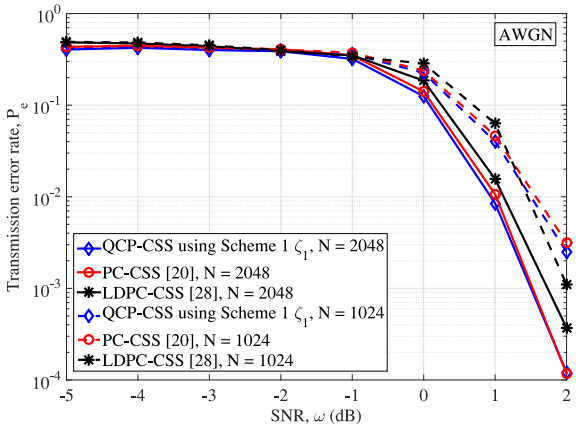

Fig. 7. The transmission error rate over AWGN channel under different N values.

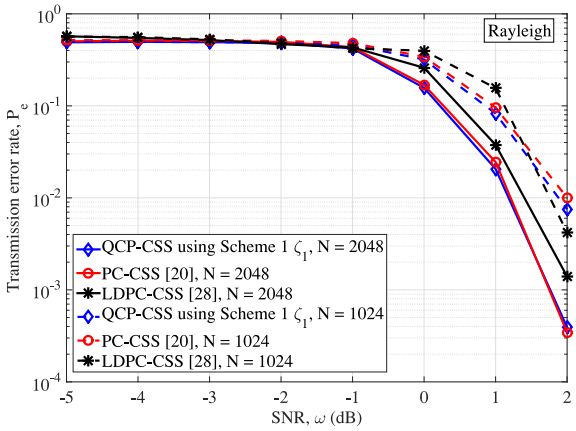

Fig. 8. The transmission error rate over Rayleigh fading channel under different N values.

$K_{\zeta_1} = P$, $K_{\zeta_2} = P + \mathtt{L}(\mathtt{D2B}(i))$, $K_{\zeta_3} = P + \mathtt{L}(\mathtt{D2B}(i)) + \mathtt{L}(\mathtt{D2B}(o_i))$ and $K_{\zeta_4} = P + \mathtt{L}(\mathtt{D2B}(i)) + \mathtt{L}(\mathtt{D2B}(a_i)) + \mathtt{L}(\mathtt{D2B}(o_i))$, where P is the length of $\mathbf{R}_i$ given in Eq. (4), $Q \times e$ is the length of the uncompressed local decision $\mathbf{S}_i$ in Eq. (4). As shown in Table I, it can be observed that for the same coding rate r, the coding complexity of Case 1 is the highest and the number of information bits is the largest, since no compressing operations are performed on bits. By contrast, in Case 2, for the same r, the QCP-CSS using Scheme 1 achieves the lowest complexity and the highest ESE. Additionally, in Case 3, it is worth mentioning that the QCP-CSS using Scheme 1, Scheme 2, and Scheme 3 will add the additional complexity to FC to generate the frozen bits, while Scheme 4 will not.

V. Simulation

In this section, simulation results are provided to demonstrate the benefits of the proposed QCP-CSS scheme. In the simulations, the parameters are set as, $M = 64$, $Q = 512$, the length of the local sensing report P is 384, the QSD level E is 8, the PU occupancy rate β_{PU} is 0.1, the sampling frequency for the energy detector f_s is 5MHz. In addition, we assume that the binary phase shift keying (BPSK) is employed.

A. Transmission Error Rate Performances of the Proposed Scheme

Firstly, we validate the effectiveness of the presented theoretical analysis via simulations. Fig. 6 illustrates the transmission error rate P_e of the proposed QCP-CSS scheme using Scheme 1 ζ_1 when the code length is $N = 1024$, $K = 410$ and the coding rate is set as 0.4. As shown in Fig. 6(a) and Fig. 6(b), over both AWGN channel and Rayleigh fading channel, we can observe that along with the increasing SNR, the transmission error rate P_e decreases. Meanwhile, it can be observed that the simulation result is higher than the lower bound given by Eq. (21) and lower than the higher bound given by Eq. (20) obtained from the Heuristic method. In addition, we can also notice that using the GA method, more accurate theoretical transmission error rate results P_e^{GA} expressed by Eq. (26) could be obtained.

B. Comparisons of Transmission Error Performances

1) Comparison With Benchmark Schemes: Fig. 7 and Fig. 8 compare the transmission error rate P_e among the proposed QCP-CSS scheme, polar-coded CSS (PC-CSS) scheme with the frozen bits set to 0 [20], and low-density parity-check coded CSS (LDPC-CSS) [28] scheme when different code length N is used over AWGN and Rayleigh fading channels using Scheme 1 ζ_1. For $K = 384$, the LDPC encoding parameters are (2048, 13, 16) and (1024, 5, 8) when N is 2048 and 1024 respectively [28]. We can observe that the QCP-CSS scheme achieves lower P_e than the LDPC-CSS schemes when $N = 2048$. When N increases, the redundancy length increases, then P_e becomes lower, as also mentioned in [20].

2) Comparison Among the Proposed Four Types of Schemes: Moreover, we compare the transmission error performance using different characteristic information processing schemes over AWGN channel and Rayleigh fading channel in Fig. 9 and Fig. 10 respectively. When SNR = 3 dB, due to the decrease of information bit number K, the code rate increases. It can be observed from the figures that P_e of QCP-CSS systems using different characteristic information processing schemes increases when the code rate increases over both AWGN channel and Rayleigh fading channel, where for ζ_1, ζ_2, ζ_3 and ζ_4, the code rate are respectively

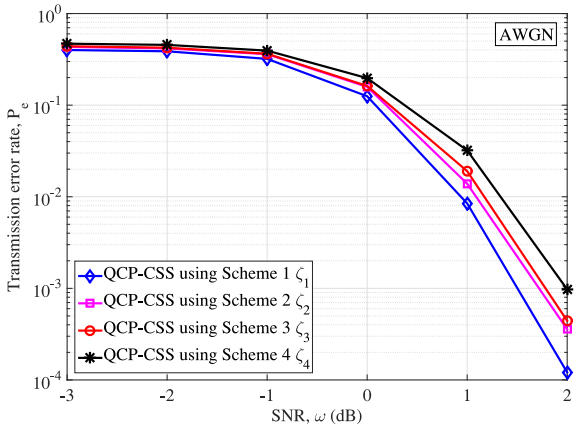

Fig. 9. The transmission error rate over AWGN channel using different characteristic information processing schemes.

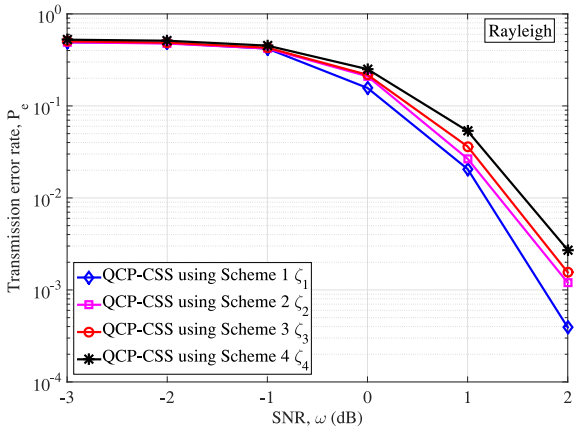

Fig. 10. The transmission error rate over Rayleigh fading channel using different characteristic information processing schemes.

$\frac{\mathtt{L}(\mathbf{R}_i)}{N}$, $\frac{\mathtt{L}(\mathbf{R}_i)+\mathtt{L}(\mathtt{D2B}(i))}{N}$, $\frac{\mathtt{L}(\mathbf{R}_i)+\mathtt{L}(\mathtt{D2B}(i))+\mathtt{L}(\mathtt{D2B}(o_i))}{N}$ and $\frac{\mathtt{L}(\mathbf{R}_i)+\mathtt{L}(\mathtt{D2B}(i))+\mathtt{L}(\mathtt{D2B}(o_i))+\mathtt{L}(\mathtt{D2B}(a_i))}{N}$. The reason is that for Scheme 1 ζ_1, all the characteristic information of SUs is encoded as the frozen bits, thus more redundancy bits are transmitted to protect the local sensing results $\mathbf{R}_i$ in the encoded data with N bits. By contrast, for Scheme 4 ζ_4, the characteristic information is regarded as information bits, thus fewer bits in the encoded data are used to correct the transmission errors, hence leading to a relatively higher transmission error rate P_e.

C. Comparisons of the Overall Detection Probability Performances

1) Comparison With Benchmark Schemes: In Fig. 11, we compare the overall detection probability performances when using the proposed scheme and the OR rule based ON/OFF reporting scheme [11] which only improves the reporting processing without the consideration of underused bands. It can be observed that based on the same SNR ω, when the overall false alarm probability Q_f is lower than 0.1, our presented QCP-CSS scheme can achieve higher overall detection probability Q_d, thereby effectively enhancing the spectrum sensing performances.

Fig. 12 and Fig. 13 illustrate the overall detection probability Q_d of underlay/overlay CRN when $N = 2048$ using

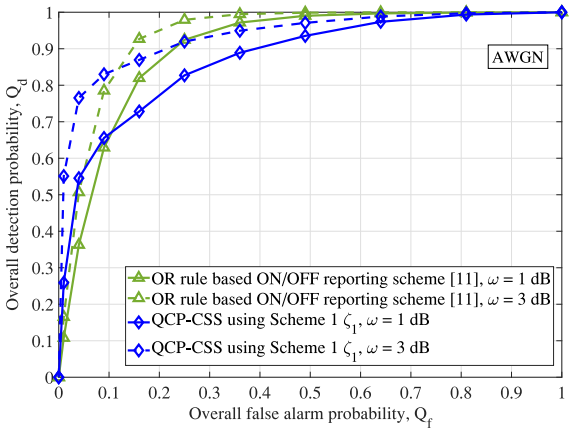

Fig. 11. The overall detection probability performance comparison between the proposed scheme and the ON/OFF reporting scheme [11] over AWGN channels in the overlay scenario.

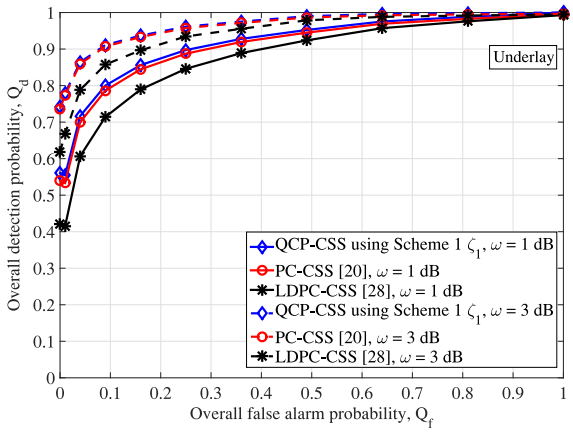

Fig. 12. The overall detection probability performance comparison among the proposed scheme, the PC-CSS scheme [20] and the LDPC-CSS scheme [28] scheme in the underlay scenario.

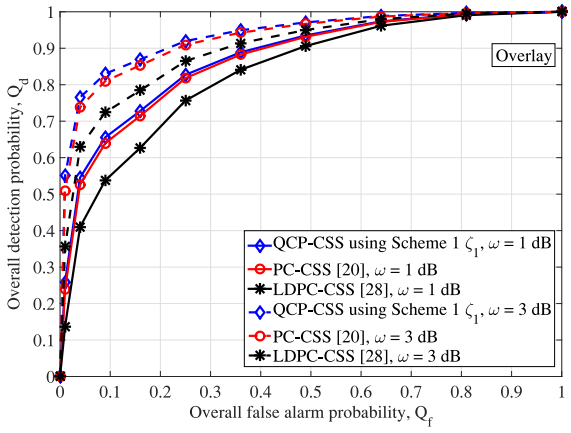

Fig. 13. The overall detection probability performance comparison among the proposed scheme, the PC-CSS scheme [20] and the LDPC-CSS scheme [28] scheme in the overlay scenario.

Scheme 1 ζ_1. We can observe that the QCP-CSS scheme achieves outstanding performances in both underlay and overlay CRNs, and Q_d is higher than that of LDPC-CSS scheme [28]. In addition, we can see that when the SNR increases, the Q_d becomes higher when Q_f remains the same.

2) Comparison Among the Proposed Four Types of Schemes: Additionally, we compare overall detection

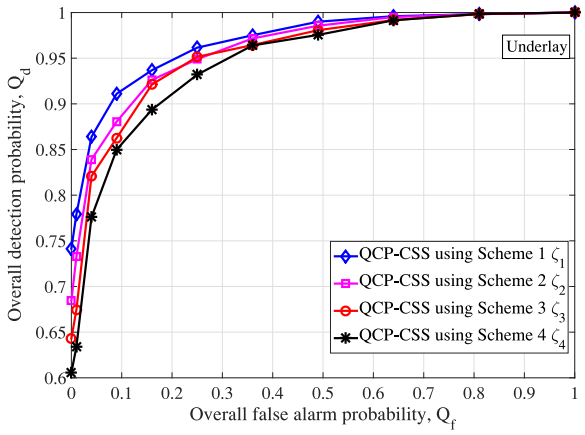

Fig. 14. The overall detection probability performances in underlay scenario when using different characteristic information processing schemes.

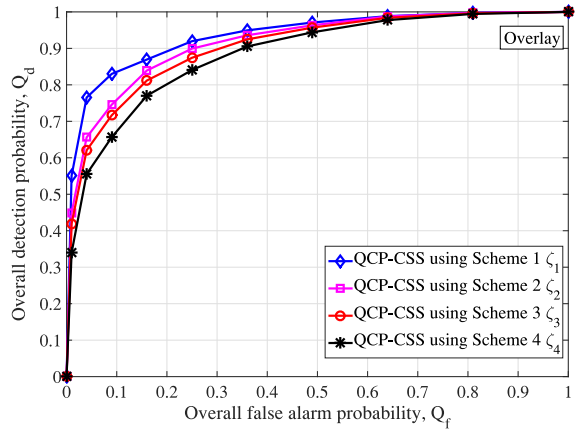

Fig. 15. The overall detection probability performances in overlay scenario when using different characteristic information processing schemes.

probability performances of QCP-CSS systems using different characteristic information processing schemes in the underlay and overlay scenario in Fig. 14 and Fig. 15 respectively. It can be observed that in both the underlay and the overlay scenario, P_e increases when the code rate increases, since the lower P_e can lead to the higher Q_d, thus Q_d becomes higher when the code rate increases. For example, when Scheme 1 ζ_1 is used, as mentioned above, all the characteristic information are treated as frozen bits, which has the lowest code rate among the four characteristic information processing schemes, thus the QCP-CSS system can achieve the best Q_d thanks to the lowest P_e as shown in Fig. 9 and in Fig. 10.

D. Comparisons of the Collision Probability Performances

1) Comparison With Benchmark Schemes: Fig. 16 and Fig. 17 illustrate the collision probability P_c of QCP-CSS aided CRNs using Scheme 1 ζ_1. It can be seen that the QCP-CSS scheme achieves the lowest P_c compared with counterpart schemes. The reason is that utilizing the cooperative characteristic information embedded into the information bits or frozen bits in the encoded data, the FC in QCP-CSS system can determine the spectrum usage status more precisely, while the PC-CSS and LDPC-CSS scheme cannot utilize any characteristic information delivered from other

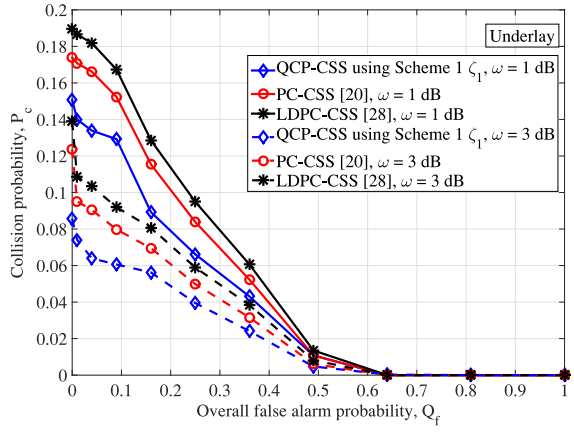

Fig. 16. The collision probability performances in underlay scenario.

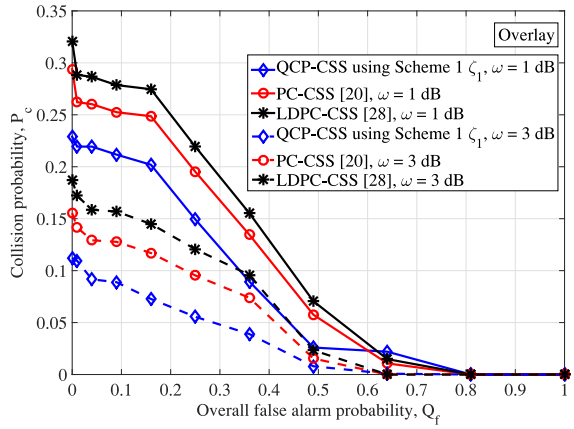

Fig. 17. The collision probability performances in overlay scenario.

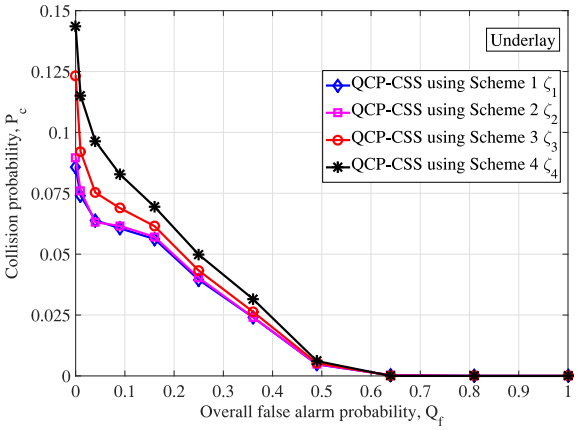

Fig. 18. The collision probability performances in the underlay scenario when using different characteristic information processing schemes.

SUs. Meanwhile, we can observe that P_c decreases when Q_f increases, which is in accordance with the conclusion given by [2].

2) Comparison Among the Proposed Four Types of Schemes: Fig. 18 and Fig. 19 provide the collision probability P_c of underlay and overlay CRNs when different characteristic information processing schemes are used. When SNR $= 3$ dB, it can be seen in Fig. 18 that the QCP-CSS system using Scheme 1 ζ_1 and Scheme 2 ζ_2 can achieve the lowest P_c

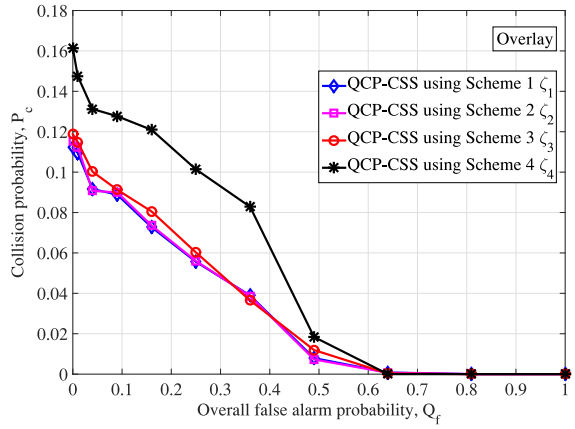

Fig. 19. The collision probability performances in the overlay scenario when using different characteristic information processing schemes.

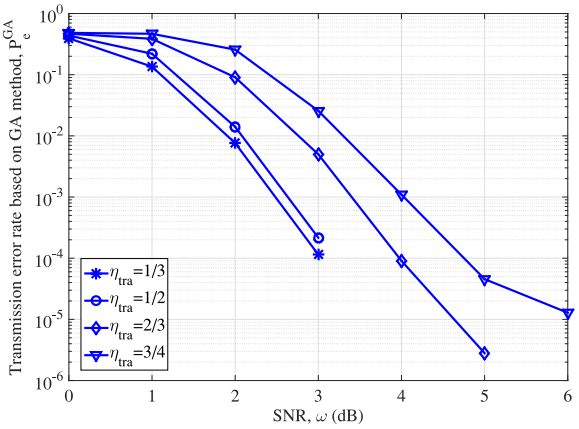

Fig. 20. Tradeoff between the reliability and traditional spectral efficiency for Scheme 4.

compared with counterpart systems using Scheme 3 ζ_3 and Scheme 4 ζ_4. The reason is that utilizing the cooperative characteristic information delivered, the FC in QCP-CSS system can determine the spectrum usage status more precisely. By contrast, for the QCP-CSS system using Scheme 3 ζ_3, no information related to the tolerance level of other SUs is delivered to FC, and the QCP-CSS system using Scheme 4 ζ_4 will not deliver any characteristic information of SUs to the FC. Since FC could not learn such information closely related to the spectrum usage status of SUs, the collision probability will increase.

Moreover, when Scheme 2 ζ_2 is used, the characteristic information o_i and a_i is embedded into the frozen bits to choose a specific sub-band, hence P_c of the QCP-CSS systems using Scheme 1 ζ_1 and Scheme 2 ζ_2 are similar. However, since in Scheme 2 ζ_2, no SU index i is delivered, hence in underlay CRNs, each SU needs to carefully identify the available sub-bands and to avoid accessing any sub-band a_i, which will reduce spectrum utilization in underlay CRNs. In addition, in the overlay scenario, the characteristic information o_i is useless, therefore, in Fig. 19 we can observe that in overlay CRNs, the collision probability of the system using Scheme 3 ζ_3 is similar with the one using Scheme 2 ζ_2.

E. The Overall Performance Comparisons Among Four Types of Schemes

As mentioned above, we propose to utilize the characteristic parameters to enhance the reliability with four types of schemes. However, the improvement of transmission reliability might be achieved at the cost of higher complexity, hence there exists the tradeoff between the traditional spectral efficiency and the reliability.

Next, we take Scheme 4 as an example to illustrate the tradeoff between the sensing performance and the spectral efficiency. For $N = 512$, as shown in Fig. 20, when the traditional spectral usage efficiency η_{tra} increases, i.e., the coding rate increases, the transmission error rate P_e^{GA} obtained from Eq. (26) increases for the same SNR.

Moreover, Table II compares the QCP-CSS systems using the four characteristic information processing schemes in terms of the transmission error rate, the overall detection probability and the collision probability. Among these four schemes, the system using Scheme 1 ζ_1 achieves the highest overall detection probability, while the system using Scheme 4 ζ_4 has the lowest complexity since no $\mathbf{u}_{A^c}^{(i)}$ is required to be updated and reported to the FC, however, its collision probability is the highest. In addition, the spectrum usage status decision precision of systems using Scheme 2 ζ_2 and Scheme 3 ζ_3 is worse than those using Scheme 1 ζ_1 and better than those using Scheme 4 ζ_4. In practical CRNs, the presented design can provide a flexible solution for the reporting information transmissions, and there exists the tradeoff between the detection performance and the complexity.

TABLE II
THE PERFORMANCE COMPARISONS OF QCP-CSS SYSTEMS USING FOUR DIFFERENT CHARACTERISTIC INFORMATION PROCESSING SCHEMES

Scheme	ζ_1	ζ_2	ζ_3	ζ_4
Embedded characteristic information number	3	2	1	0
Example	i, o_i, a_i	o_i, a_i	a_i	None
C_i needs to update $\mathbf{u}_{A^c}^{(i)}$ to FC	✓	✓	✓	×
C_i accesses to spectrum based on $\mathbf{u}_{A^c}$	✓	✓	✓	×
Transmission complexity	$\zeta_1 > \zeta_2 > \zeta_3 > \zeta_4$			
Transmission error rate, P_e	$\zeta_1 < \zeta_2 < \zeta_3 < \zeta_4$			
Overall detection probability, Q_d	$\zeta_1 > \zeta_2 > \zeta_3 > \zeta_4$			
Collision probability, P_c	Underlay: $\zeta_1 \approx \zeta_2 < \zeta_3 < \zeta_4$ Overlay: $\zeta_1 \approx \zeta_2 \approx \zeta_3 < \zeta_4$			

VI. CONCLUSION

In this paper, we propose a novel QCP-CSS scheme to provide a general QSD-based compressive local sensing report method with adjustable quantization levels for hybrid underlay and overlay CRNs. Different from the traditional research works which did not consider the hybrid underlay and overlay spectrum usage scenario and little research has been conducted on the reporting of different spectrum usage status, we propose to quantize the spectrum sensing results, then they are compressed to be transmitted over a polarized channel. Notably, during the polarization transmission, the sensing results are regarded as information bits, while the whole or a part of SU characteristic information, which includes the SU index, the interference tolerance level, and the accessed sub-band index,

are treated as frozen bits. Thus the transmission reliability of sensing results is enhanced, thereby improving the spectrum usage efficiency and reducing the collision probability. Then both parts are embedded into the encoded data using four types of schemes. Simulation results obtained in underlay/overlay scenarios over AWGN/Rayleigh fading channels validate our theoretical analysis and demonstrate that our scheme outperforms counterpart schemes in terms of the transmission error rate, the overall detection probability, and the collision probability. Last but not the least, it is worth pointing out future research works could be extended to investigate the behaviors of the malicious or greedy SUs who always occupy the spectrum bands, and then the security and sensing performances could be potentially further improved.

REFERENCES

[1] J. Zou, H. Xiong, D. Wang, and C. W. Chen, "Optimal power allocation for hybrid overlay/underlay spectrum sharing in multiband cognitive radio networks," *IEEE Trans. Veh. Technol.*, vol. 62, no. 4, pp. 1827–1837, May 2013.

[2] K. Cichoń, A. Kliks, and H. Bogucka, "Energy-efficient cooperative spectrum sensing: A survey," *IEEE Commun. Surveys Tuts.*, vol. 18, no. 3, pp. 1861–1886, 3rd Quart., 2016.

[3] M. E. Tanab and W. Hamouda, "Resource allocation for underlay cognitive radio networks: A survey," *IEEE Commun. Surveys Tuts.*, vol. 19, no. 2, pp. 1249–1276, 2nd Quart., 2017.

[4] N. Nguyen-Thanh and I. Koo, "Log-likelihood ratio optimal quantizer for cooperative spectrum sensing in cognitive radio," *IEEE Commun. Lett.*, vol. 15, no. 3, pp. 317–319, Mar. 2011.

[5] B. Kailkhura, T. Wimalajeewa, and P. K. Varshney, "Collaborative compressive detection with physical layer secrecy constraints," *IEEE Trans. Signal Process.*, vol. 65, no. 4, pp. 1013–1025, Feb. 2017.

[6] S. Chaudhari, J. Lunden, V. Koivunen, and H. V. Poor, "Cooperative sensing with imperfect reporting channels: Hard decisions or soft decisions?" *IEEE Trans. Signal Process.*, vol. 60, no. 1, pp. 18–28, Jan. 2012.

[7] A. Dehghani Firouzabadi and A. M. Rabiei, "Sensing-throughput optimisation for multichannel cooperative spectrum sensing with imperfect reporting channels," *IET Commun.*, vol. 9, no. 18, pp. 2188–2196, Dec. 2015.

[8] J. W. Lee, "Cooperative spectrum sensing scheme over imperfect feedback channels," *IEEE Commun. Lett.*, vol. 17, no. 6, pp. 1192–1195, Jun. 2013.

[9] C. Wang, T. Song, J. Wu, Y. Yu, and J. Hu, "Energy-efficient cooperative spectrum sensing with reporting errors in hybrid spectrum sharing CRNs," *IEEE Access*, vol. 6, pp. 48391–48402, 2018.

[10] M. Ben Ghorbel, H. Nam, and M. Alouini, "Soft cooperative spectrum sensing performance under imperfect and non identical reporting channels," *IEEE Commun. Lett.*, vol. 19, no. 2, pp. 227–230, Feb. 2015.

[11] S. Bae and H. Kim, "Robust cooperative sensing with ON/OFF signaling over imperfect reporting channels," *IEEE Trans. Ind. Informat.*, vol. 12, no. 6, pp. 2196–2205, Dec. 2016.

[12] X. Wu, L. Zhang, and M. Jiang, "Priority-based polarized transmission for feedback channels in cooperative spectrum sensing systems," *IEEE Commun. Lett.*, vol. 22, no. 4, pp. 836–839, Apr. 2018.

[13] Z. Tian and G. B. Giannakis, "Compressed sensing for wideband cognitive radios," in *Proc. IEEE Int. Conf. Acoust. Speech Signal Process. (ICASSP)*, vol. 4. Honolulu, HI, USA, Apr. 2007, pp. 1357–1360.

[14] H. Zhuang, Z. Luo, J. Zhang, and H. Yanikomeroglu, "Hierarchical and adaptive spectrum sensing in cognitive radio based multi-hop cellular networks," in *Proc. IEEE 72nd Veh. Technol. Conf. Fall*, Ottawa, ON, Canada, Sep. 2010, pp. 1–6.

[15] A. Bhowmick, M. Dolly, S. D. Roy, and S. Kundu, "Power control with rank based censoring in cognitive radio network," in *Proc. Int. Conf. Devices Circuits Commun.*, Ranchi, India, Jan. 2014, pp. 1–6.

[16] R. Alhamad, H. Wang, and Y.-D. Yao, "Cooperative spectrum sensing with random access reporting channels in cognitive radio networks," *IEEE Trans. Veh. Technol.*, vol. 66, no. 8, pp. 7249–7261, Aug. 2017.

[17] V. Chakravarthy *et al.*, "Novel overlay/underlay cognitive radio waveforms using SD-SMSE framework to enhance spectrum efficiency- part I: Theoretical framework and analysis in AWGN channel," *IEEE Trans. Commun.*, vol. 57, no. 12, pp. 3794–3804, Dec. 2009.

[18] T. A. Le and K. Navaie, "On the interference tolerance of the primary system in cognitive radio networks," *IEEE Wireless Commun. Lett.*, vol. 4, no. 3, pp. 281–284, Jun. 2015.

[19] V. Chakravarthy, Z. Wu, M. Temple, X. Li, and R. Zhou, "Novel overlay/underlay cognitive radio waveforms using SD-SMSE framework to enhance spectrum efficiency-part II: Analysis in fading channel," *IEEE Trans. Commun.*, vol. 58, no. 6, pp. 1868–1876, Jun. 2010.

[20] E. Arikan, "Channel polarization: A method for constructing capacity-achieving codes for symmetric binary-input memoryless channels," *IEEE Trans. Inf. Theory*, vol. 55, no. 7, pp. 3051–3073, Jul. 2009.

[21] D. Zhou, K. Niu, and C. Dong, "Construction of polar codes in Rayleigh fading channel," *IEEE Commun. Lett.*, vol. 23, no. 3, pp. 402–405, Mar. 2019.

[22] D. Messerschmitt, "Quantizing for maximum output entropy (corresp.)," *IEEE Trans. Inf. Theory*, vol. 17, no. 5, p. 612, Sep. 1971.

[23] D. L. Donoho, "Compressed sensing," *IEEE Trans. Inf. Theory*, vol. 52, no. 4, pp. 1289–1306, Apr. 2006.

[24] R. Kishore, S. Gurugopinath, S. Muhaidat, P. C. Sofotasios, M. Dianati, and N. Al-Dhahir, "Energy efficiency analysis of collaborative compressive sensing for cognitive radio networks," in *Proc. IEEE Global Commun. Conf. (GLOBECOM)*, Abu Dhabi, UAE, Dec. 2018, pp. 1–6.

[25] S. S. Chen, D. L. Donoho, and M. A. Saunders, "Atomic decomposition by basis pursuit," *SIAM Rev.*, vol. 43, no. 1, pp. 129–159, Jan. 2001.

[26] C. Zhang and K. K. Parhi, "Low-latency sequential and overlapped architectures for successive cancellation polar decoder," *IEEE Trans. Signal Process.*, vol. 61, no. 10, pp. 2429–2441, May 2013.

[27] H. Li and J. Yuan, "A practical construction method for polar codes in AWGN channels," in *Proc. IEEE Tencon Conf. Spring*, Sydney, NSW, Australia, Apr. 2013, pp. 223–226.

[28] A. G. Dimakis, R. Smarandache, and P. O. Vontobel, "LDPC codes for compressed sensing," *IEEE Trans. Inf. Theory*, vol. 58, no. 5, pp. 3093–3114, May 2012.

Xiaoge Wu (Graduate Student Member, IEEE) received the B.S. degree in communication engineering from Sun Yat-sen University, Guangzhou, China, in 2016, where she is currently pursuing the Doctoral degree in information and communication engineering. Her research interests include chaotic communication, polar codes, cognitive radio, and intelligent communications.

Lin Zhang (Senior Member, IEEE) received the B.S. and M.S. degrees in electrical engineering from Shanghai University in 1997 and 2000, respectively, and the Ph.D. degree in electrical engineering from Sun Yat-sen University in 2003, where she joined the Department of Electrical Engineering in 2003, and has been served as an Associate Professor since 2007. From 2008 to 2009, she was a visiting researcher with the Electrical and Computer Engineering Department, University of Maryland, College Park, MD, USA, for one year. Since 2016, she has been with the School of Electronics and Information Technology, Sun Yat-sen University, and also cooperate with Shandong Provincial Key Laboratory of Wireless Communication Technologies. Her research has been supported by National Natural Science Foundation of China and the Science and Technology Program Project of Guangdong Province. Her current research interests are in the area of signal processing and their applications to wireless communication systems.

Zhiqiang Wu (Senior Member, IEEE) received the B.S. degree in electrical engineering from the Beijing University of Posts and Telecommunications in 1993, the M.S. degree in electrical engineering from Peking University in 1996, and the Ph.D. degree in electrical engineering from Colorado State University in 2002. He served as an Assistant Professor with the Department of Electrical and Computer Engineering, West Virginia University Institute of Technology, from 2003 to 2005. He joined Wright State University in 2005 where he currently serves as a Full Professor with the Department of Electrical Engineering. His research has been supported by NSF, AFRL, ONR, AFOSR and OFRN. He has also held visiting positions with Peking University, Harbin Engineering University, Guizhou Normal University, and Tibet University.